Gammaherpesvirus-mediated repression reveals EWSR1 to be a negative regulator of B cell responses

Yiping Wang[a,b,c] (iD), April Feswick[a,b,c], Vasiliki Apostolou[a,b,c] (iD), Petko M. Petkov[d] (iD), Emily K. Moser[e,f] (iD), and Scott A. Tibbetts[a,b,c,1] (iD)

The germinal center (GC) plays a central role in the generation of antigen-specific B cells and antibodies. Tight regulation of the GC is essential due to the inherent risks of tumorigenesis and autoimmunity posed by inappropriate GC B cell processes. Gammaherpesviruses such as Epstein–Barr virus (EBV) and murine gammaherpesvirus 68 (MHV68) utilize numerous armaments to drive infected naïve B cells, independent of antigen, through GC reactions to expand the latently infected B cell population and establish a stable latency reservoir. We previously demonstrated that the MHV68 microRNA (miRNA) *mghv-miR-M1-7-5p* represses host *EWSR1* (Ewing sarcoma breakpoint region 1) to promote B cell infection. EWSR1 is a transcription and splicing regulator that is recognized for its involvement as a fusion protein in Ewing sarcoma. A function for EWSR1 in B cell responses has not been previously reported. Here, we demonstrate that 1) B cell–specific deletion of EWSR1 had no effect on generation of mature B cell subsets or basal immunoglobulin levels in naïve mice, 2) repression or ablation of EWSR1 in B cells promoted expansion of MHV68 latently infected GC B cells, and 3) B cell–specific deletion of EWSR1 during a normal immune response to nonviral antigen resulted in significantly elevated numbers of antigen-specific GC B cells, plasma cells, and circulating antibodies. Notably, EWSR1 deficiency did not affect the proliferation or survival of GC B cells but instead resulted in the generation of increased numbers of precursor GC B cells. Cumulatively, these findings demonstrate that EWSR1 is a negative regulator of B cell responses.

B cell | germinal center | EWSR1 | herpesvirus | lymphoma

The germinal center (GC) is a specific histological structure that forms within peripheral lymphoid organs in response to antigen stimulation. Upon antigen-specific activation, naïve follicular B cells enter the GC, where B cells with appropriate high affinity for antigen are positively selected for expansion and further differentiation into antibody-secreting plasma cells and/or memory B cells. This process is governed by a tightly regulated network of signaling pathways and transcription factors, including BCL6, NF-κB, and IRF4 (reviewed in refs. 1–4). Thus, the GC represents the central avenue through which humoral immune responses are generated. Notably though, the crucial genetic processes that are fundamental to GC B cell biology, immunoglobulin somatic hypermutation and class-switch recombination, provide a fertile ground for secondary mutations that can drive the malignant transformation of B cells (1, 2, 5, 6). Not surprisingly then, a large majority of B cell malignancies, including gammaherpesvirus-associated lymphomas, are derived from GC B cells (1–4). Similarly, the genesis of many autoimmune disorders lies in the dysregulation of GC B cell responses (7). Therefore, biological mechanisms that tightly regulate B cell differentiation and selection are critical for maintaining normal GC homeostasis and preventing GC B cell–based diseases.

The human gammaherpesviruses Epstein–Barr virus (EBV) and Kaposi's sarcoma–associated herpesvirus (KSHV) are ubiquitous pathogens that directly contribute to the development of numerous types of malignances, including numerous B cell lymphomas that originate in the GC (8–10). A hallmark of these viruses is their ability to establish latent infection in circulating B cells, a step which is requisite for both lifelong infection and lymphomagenesis (11, 12). However, the precise underlying mechanisms by which they establish latency in the B cell compartment and induce B cell lymphoma in vivo remain poorly understood due to their strict species restriction (11, 12). Murine gammaherpesvirus 68 (MHV68, MuHV-4, γHV68) is a natural pathogen of murid rodents that is genetically and pathogenically related to EBV and KSHV (11–13). Like the human gammaherpesviruses, MHV68 establishes chronic latent infection in the B cell compartment (11, 12) and is directly associated with the development of B cell lymphoproliferative diseases and lymphomas (14, 15), and thus offers a highly tractable system for defining in vivo mechanisms by which gammaherpesviruses establish infection and cause disease.

The GC plays a central role in gammaherpesvirus biology. For example, EBV is thought to initially infect naïve B cells and then, independent of antigen, drive these infected cells

Significance

The germinal center (GC) is an important histological structure that plays a central role in the generation of immune responses, including antigen-specific B cells and antibodies. Tight regulation of the GC is essential due to the inherent risks of tumorigenesis and autoimmunity posed by inappropriate GC B cell expansion and differentiation. EWSR1 (Ewing sarcoma breakpoint region 1) is a multifunctional host protein that has no known role in B cells. Here, we demonstrate that repression or deletion of EWSR1 promoted GC B cell responses both during gammaherpesvirus infection and in normal immune responses outside of the context of infection. Cumulatively, these findings demonstrate that EWSR1 is a negative regulator of B cell responses.

into the GC, where they undergo proliferative expansion before differentiating into long-lived, resting memory B cells (8, 16, 17). Consistent with this concept, MHV68 is preferentially maintained in GC B cells during the expansion phase of latency (18–20). Thus, it is not surprising that these viruses employ multiple molecular mechanisms to manipulate GC B cell biology. Among the array of armaments utilized by these viruses to manipulate host cells are microRNAs (miRNAs), short noncoding regulatory RNA molecules that posttranscriptionally regulate gene expression through binding to complementary cognate sequences within messenger RNA (mRNA) target transcripts, resulting in silencing of mRNA targets (21, 22). We have previously demonstrated that the MHV68 precursor miRNA (pre-miR) *pre-miR-7* of the *TMER5* gene is required for efficient establishment of latency in GC B cells in vivo (23). Through a cutting-edge miRNA target identification approach, we identified *EWSR1* (EWSR1/EWS; Ewing sarcoma breakpoint region 1) as the most prominent host mRNA target for MHV68 *mghv-M1-miR-7-5p* in infected cells. Importantly, expression of anti-*EWSR1* short hairpin RNAs (shRNAs) in place of *pre-miR-7* fully rescued the attenuation of *pre-miR-7*–deficient virus in vivo, demonstrating a critical role for EWSR1 repression during MHV68 infection of B cells in vivo (23).

Thus, these findings were notable because they implied a key role for EWSR1 in regulation of GC B cells, at least in the context of gammaherpesvirus infection. EWSR1, along with FUS/TLS and TAF15, are members of the FET family of proteins (24). EWSR1 is widely recognized in cancer biology for the contribution of its transcription-activating domain to the oncogenic fusion protein EWS/FLI-1, which drives transformation in Ewing's sarcoma (25, 26). In its native form, EWSR1 is composed of a 5′ intrinsically disordered transactivation domain and a 3′ RNA/DNA–binding region (25). Native EWSR1 has been reported to carry out a very wide range of context-dependent actions, including transcriptional activation, transcriptional repression, and RNA binding, to influence splicing and mRNA transport (27, 28). For example, in stress responses, EWSR1 regulates both gene expression and alternative splicing of DNA damage response–associated genes (29–31).

To date, EWSR1 has no known function in mature B cell biology. In the work described here, we utilize *EWSR1* conditional knockout (CKO) mice to further examine the role of EWSR1 in GC B cells during chronic MHV68 infection, and to define whether EWSR1 plays a regulatory role in nonviral antigen-mediated immune responses. Through systemic in vivo investigations, we demonstrate that 1) reduction or loss of EWSR1 expression in mice significantly expands the infected GC B cell population during MHV68 latency, and 2) EWSR1 deficiency in B cells results in significantly elevated antigen-specific GC B cell and class-switched antibody responses during a T cell–dependent immune response. EWSR1 deficiency did not affect the development of mature B cells, or the proliferation and survival of GC B cells, but instead significantly enhanced the generation of precursor GC (Pre-GC) B cells. Taken together, these findings demonstrate that EWSR1 functions as a molecular brake to constrain both gammaherpesvirus-driven and nonviral antigen-mediated GC B cell responses.

Results

Gammaherpesvirus-Mediated Repression of EWSR1 Promotes Expansion of the Infected GC B Cell Compartment. As described above, we have previously demonstrated that MHV68 represses *EWSR1* to significantly enhance GC B cell infection in vivo (23). To determine whether this enhanced infection was apparent throughout the proliferative expansion phase of the GC reaction, we first generated MHV68 recombinant viruses expressing 1) anti-*EWSR1* shRNAs (MHV68.YFP.EWshR) or control scrambled sequence shRNAs (MHV68.YFP.SCshR) in place of *pre-miR-7* and *pre-miR-12* stem loops (Fig. 1*A*), and 2) enhanced yellow fluorescent protein (eYFP) under the control of the H2b promoter. The eYFP-expressing genome is phenotypically wild-type (WT) but eYFP expression can be used to facilitate identification of infected cells from in vivo samples (18).

To verify that MHV68-expressing anti-*EWSR1* shRNAs could specifically repress *EWSR1* transcript expression in latently infected GC B cells in vivo, we infected WT C57BL/6J (B6) mice intranasally (i.n.) and quantified *EWSR1* expression in GC B cells during latency establishment. At 16 d post infection (dpi), splenocytes were harvested, and B cells were isolated by immunomagnetic negative selection and then stained for GC B cell-surface markers CD19, GL7, and CD95. Subsequently, infected GC B cells were flow cytometrically sorted based on CD19+ GL7+ CD95+ YFP+ gating (Fig. 1*B*). Following extraction of RNA from sorted GC B cells, *EWSR1* mRNA expression level was quantified by qRT-PCR (Fig. 1*C*). Consistent with our previous demonstration that *TMER5*-derived *miR-7-5p* suppresses *EWSR1* (23), GC B cells infected with recombinant virus carrying scrambled shRNAs in place of *TMER5* pre-miRNA stem loops (SC.shR) displayed significantly increased levels of *EWSR1* transcript in comparison with GC B cells infected with WT MHV68. In contrast, *EWSR1* expression in GC B cells infected with recombinant virus carrying anti-*EWSR1* shRNAs in place of *TMER5* pre-miRNA stem loops (EW.shR) was restored to a level at or below that of WT virus, demonstrating that virus-encoded anti-*EWSR1* shRNAs effectively suppress *EWSR1* transcript levels in vivo.

To test whether selective repression of *EWSR1* promoted increased numbers of infected GC B cells during latency, we infected mice with MHV68.YFP.WT, MHV68.YFP.SCshR, or MHV68.YFP.EWshR viruses for 16 d, and then quantified the absolute number of YFP+ GC B cells present in the spleen using flow cytometry (Fig. 1*D*). In accordance with our previous findings (23), the number of GC B cells (CD19+ GL7+ CD95+ YFP+) infected with the *pre-miR-7*–deficient virus expressing scrambled shRNAs was reduced more than 27-fold (WT, 38,470; SC.shR, 1,420). In contrast, incorporation of anti-*EWSR1* shRNAs into the *pre-miR-7*–deficient virus resulted in nearly complete restoration of GC B cell infection to levels equivalent to that of WT virus (WT, 38,470; EW.shR, 25,250). Thus, these findings confirmed that shRNA-mediated selective repression of *EWSR1* in vivo promotes MHV68 infection of GC B cells during latency establishment.

We next determined whether the increased numbers of infected GC B cells observed in the context of *EWSR1* repression vs. derepression were apparent throughout the proliferative expansion phase of the GC reaction. B6 mice were inoculated with MHV68.YFP.WT, MHV68.YFP.SCshR, or MHV68.YFP.EWshR virus, and then the numbers of infected GC B cells were quantified by flow cytometry at 13, 16, and 19 dpi (Fig. 1*E*). Notably, while the number of GC B cells infected with either WT virus or *pre-miR-7*–deficient virus expressing anti-*EWSR1* shRNAs expanded significantly from 13 to 19 dpi, the number of GC B cells infected with *pre-miR-7*–deficient virus expressing scrambled shRNAs remained stable over time (EW.shR, 36-fold change; SC.shR, 2-fold change). Thus, collectively these findings strongly suggested that viral miRNA-mediated repression of *EWSR1* promotes expansion of the latently infected GC B cell population.
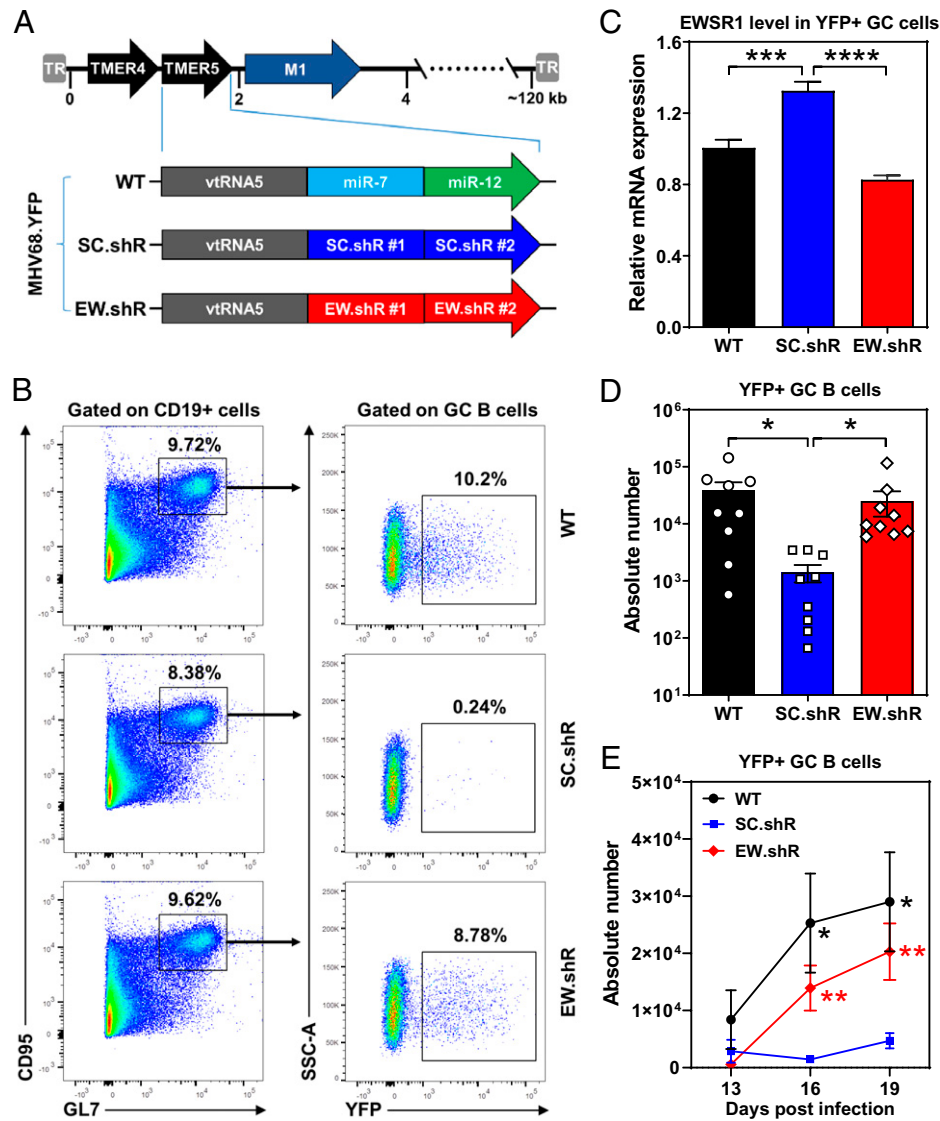
Fig. 1. shRNA-mediated selective repression of *EWSR1* in vivo promotes MHV68 infection of GC B cells. (*A*) Schematic diagram of MHV68 recombinant viruses carrying WT TMER5 (MHV68.YFP.WT) or TMER5 carrying anti-*EWSR1* shRNAs (MHV68.YFP.EWshR) or scrambled shRNAs (MHV68.YFP.SCshR) in place of *pre-miR-7* and *pre-miR-12* stem loops. Diagram depicts TMER5 gene location relative to terminal repeats (TR) and surrounding genes TMER4 and M1. (*B*) Gating strategy used for flow sorting virus-positive GC B cells using representative flow plots. C57BL/6J mice were infected i.n. with 10^4 PFUs of WT parental virus MHV68.YFP.WT, MHV68.YFP.SCshR, or MHV68.YFP.EWshR. At 16 dpi, the splenocytes were harvested, and B cells were then isolated and subjected to flow cytometric sorting for virus-positive GC B cells (CD19$^+$ GL7$^+$ CD95$^+$ YFP$^+$). (*C*) Relative expression of endogenous *EWSR1* mRNA in infected GC B cells sorted from in vivo samples. The *EWSR1* mRNA expression level in infected GC B cells from each group was determined by qRT-PCR. The values represent the means ± the SEM of two independent experiments. Significance was determined by a two-tailed, unpaired *t* test (***$P < 0.001$, ****$P < 0.0001$). (*D*) The number of virus-positive GC B cells during the peak of latency. The mice were infected as described in *B*, and the latent infection of GC B cells was quantified by using flow cytometry at 16 dpi. Each symbol represents an individual mouse. The values represent the means ± the SEM of three independent experiments. Significance was determined by a two-tailed, unpaired *t* test (*$P < 0.05$). (*E*) The number of virus-positive GC B cells during the expansion phase of latency. The mice were infected as described in *B*, then at 13, 16, and 19 dpi, splenocytes were harvested and subjected to flow cytometric quantification for virus-positive GC B cells. The values represent the means ± the SEM of two or three independent experiments. Significance was determined by a two-tailed, unpaired *t* test (*$P < 0.05$, **$P < 0.01$).

MHV68 infects multiple cell types, including B cells, macrophages, dendritic cells, and epithelial cells (11, 12). To determine whether the requirement for EWSR1 repression was intrinsic to B cell infection or instead due to effects on other cell types, we generated mice with B cell–specific deletion of *EWSR1*. Mice homozygous for loxP-flanked (floxed) *EWSR1* exon 4 (EWSR1$^{flox/flox}$ CD19$^{+/+}$; designated EWSR1 WT mice) (32, 33) were crossed with CD19-Cre mice (34) to generate CKO mice in which EWSR1 is specifically deleted in B cells (EWSR1$^{flox/flox}$ CD19$^{Cre/+}$; designated EWSR1 CKO mice) (Fig. 2*A*). Through genomic PCR for the floxed region using DNA extracted from purified B cells, we validated that *EWSR1* exon 4 flanked by two loxP sites was efficiently excised

in the EWSR1 CKO mice (Fig. 2*B*). We further confirmed that deletion of *EWSR1* exon 4 resulted in a complete loss of EWSR1 protein expression in purified B cells from EWSR1 CKO mice (Fig. 2*C*).

We next infected EWSR1 WT and CKO mice with YFP-expressing WT or *pre-miR-7*–deficient viruses for 16 d, and then quantified the GC B cell infection using flow cytometry (Fig. 2*D*). Consistent with our previous findings (23), infection of EWSR1 WT mice with the *pre-miR-7*–deficient virus resulted in a 12-fold decrease in the number of latent GC B cells (B220$^+$ GL7$^+$ CD95$^+$ YFP$^+$) as compared with WT virus (Fig. 2*E*). In contrast, the *pre-miR-7*–deficient virus displayed only a 2-fold decrease in the number of latent GC B cells in
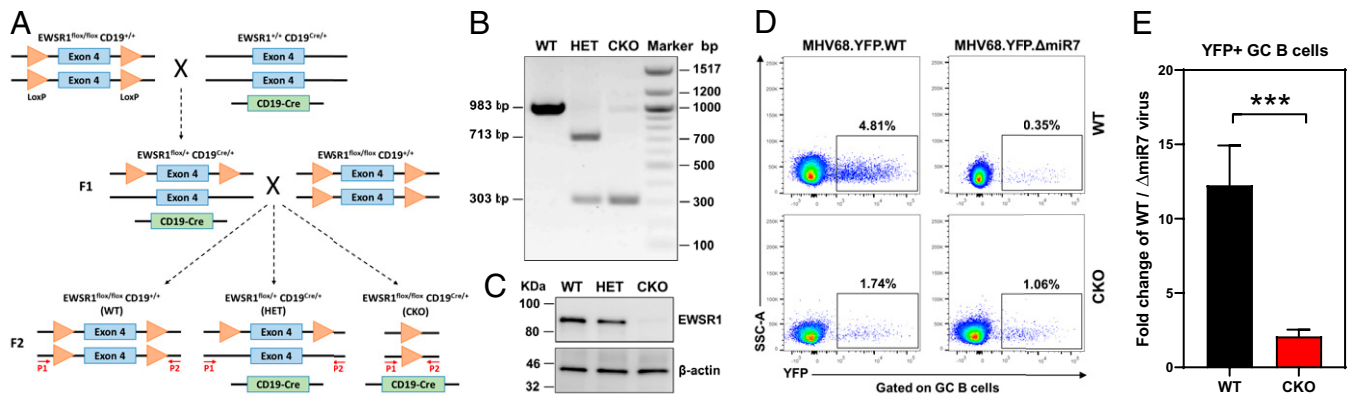
Fig. 2. B cell–specific deletion of EWSR1 in vivo promotes latent infection of GC B cells with MHV68. (*A*) Schematic diagram of a two-step breeding strategy used for generating the mice with CKO of EWSR1 in B cells. The EWSR1$^{flox/flox}$ mice were first crossed to CD19-Cre mice to generate the F1 offspring: the heterozygous EWSR1$^{flox/+}$ CD19$^{Cre/+}$ mice (designated EWSR1 HET mice). In the F2 generation, the EWSR1$^{flox/flox}$ CD19$^{Cre/+}$ mice (designated EWSR1 CKO mice) were obtained by mating the EWSR1 HET mice back to the EWSR1$^{flox/flox}$ mice. Littermate EWSR1$^{flox/flox}$ CD19$^{+/+}$ mice (designated EWSR1 WT mice) were used as controls in all experiments. Mice genotypes were identified by PCR with the primers P1 located upstream of the first loxP site and P2 located downstream of the second loxP site. (*B*) Genotyping EWSR1 CKO mice by PCR. DNA was extracted from B cells isolated from naïve mice by immunomagnetic negative selection, and PCR was then performed with the P1 and P2 primers. Length of amplicons: one band of 983 bp in EWSR1 WT mice, two bands of 713 and 303 bp in EWSR1 HET mice, and one band of 303 bp in EWSR1 CKO mice. (*C*) Validation of the EWSR1 CKO mouse genotype by Western blots. The EWSR1 protein expression level in purified B cells was determined by Western blots. β-actin was included as a loading control. (*D* and *E*) The EWSR1 WT or CKO mice were infected i.n. with 10^4 PFUs of WT parental virus MHV68.YFP.WT or the *pre-miR-7*–deficient virus MHV68.YFP.ΔmiR7. At 16 dpi, the splenocytes were harvested and subjected to flow cytometric quantification for virus-positive GC B cells (B220$^+$ GL7$^+$ CD95$^+$ YFP$^+$). (*D*) Representative flow plots for showing the gating of YFP$^+$ cells from B220$^+$ GL7$^+$ CD95$^+$ GC B cells. (*E*) Fold changes of the number of YFP$^+$ GC B cells infected with MHV68.YFP.WT virus to that of YFP$^+$ GC B cells infected with MHV68.YFP.ΔmiR7 virus in EWSR1 WT or CKO mice are shown. The values represent the means ± the SEM of three independent experiments. Significance was determined by a two-tailed, unpaired *t* test (***$P < 0.001$).

EWSR1 CKO mice (Fig. 2*E*), indicating that B cell–specific deletion of EWSR1 complemented the absence of *pre-miR-7* in MHV68-infected cells. Cumulatively, these findings demonstrate that viral repression of *EWSR1* promotes gammaherpesvirus-driven GC B cell infection.

EWSR1 Is Not Required for Normal Peripheral B Cell Development and Basal Serum Immunoglobulin Production. The function of EWSR1 in mature B cells is unknown. However, the above findings suggested that MHV68 may exploit a previously unrecognized role for EWSR1 in regulation of B cell responses to foreign antigens. To address this possibility, we used EWSR1 CKO mice to define parameters of B cell development and B cell responses to a nonviral antigen in the absence of EWSR1. To first determine whether EWSR1 is important for peripheral B cell development, we quantified the number of total B cells and B cell subsets in the spleen of naïve EWSR1 WT and CKO mice by flow cytometry (Fig. 3 *A–D*). The number of total B cells (B220$^+$ CD3$^-$) in the spleen of naïve CKO mice was nearly identical to that of naïve WT mice (Fig. 3 *A* and *B*), as was the case for the total T cell (B220$^-$ CD3$^+$) population (Fig. 3 *A* and *B*). Further, no significant differences were observed in levels of peripheral B cell subsets of CKO mice (Fig. 3 *C* and *D*), including transitional B cells (B220$^+$ CD93$^+$), follicular (FO) B cells (B220$^+$ CD93$^-$ CD23$^+$), and marginal zone (MZ) B cells (B220$^+$ CD93$^-$ CD23$^{low/-}$ CD21$^+$). Additionally, naïve CKO mice exhibited no significant difference in the number of spontaneously activated GC B cells (B220$^+$ GL7$^+$ CD95$^+$) (Fig. 3 *E* and *F*). Finally, to determine whether EWSR1 deficiency in B cells affects basal serum immunoglobulin production, we performed an enzyme-linked immunosorbent assay (ELISA) to quantify serum immunoglobulin levels in naïve EWSR1 WT or CKO mice (Fig. 3*G*). However, levels of immunoglobulin M (IgM), total IgG, IgG1, IgG2b, IgG2c, and IgG3 in naïve WT and CKO mice were nearly equivalent (Fig. 3*G*), demonstrating that B cell–specific deletion of EWSR1 does not alter basal levels of serum immunoglobulin. Thus, together, these data demonstrate

that EWSR1 is dispensable for normal development of mature peripheral B cells.

EWSR1 Restricts T Cell–Dependent Antigen-Mediated GC B Cell Responses to Limit Excessive Humoral Immunity. We next queried whether EWSR1 regulates nonviral antigen-specific GC B cell responses. To first test this possibility, EWSR1 WT and CKO mice were mock-treated, or immunized intraperitoneally (i.p.) with the T cell–dependent antigen 4-hydroxy-3-nitrophenylacetyl–keyhole limpet hemocyanin (NP-KLH). Two weeks later, splenocytes were harvested, stained for specific GC B cell-surface markers B220, GL7, and CD95, and then analyzed by flow cytometry (Fig. 4*A*). In agreement with experiments in naïve mice (Fig. 3 *E* and *F*), the number of GC B cells (B220$^+$ GL7$^+$ CD95$^+$) detected in mock-treated mice carrying B cell–specific deletion of EWSR1 was equivalent to that of mock-treated WT mice (Fig. 4 *B* and *C*), providing further evidence that EWSR1 has no effect on spontaneous activation of GC B cells. Notably though, following NP-KLH immunization, the number of GC B cells present in EWSR1 CKO mice was significantly increased as compared with that of EWSR1 WT control mice (Fig. 4 *B* and *C*). Consistent with this, in situ hybridization for the GC B cell marker *BCL6* indicated normal GC architecture but vastly expanded GC B cell zones (Fig. 4*D*). To determine whether these enhanced GC B cell responses resulted in increased numbers of antigen-specific B cells, we quantified NP-specific GC B cells using fluorescently labeled NP antigen in conjunction with GC B cell-surface markers (Fig. 4 *E–G*). Indeed, in parallel with the overall increase in total GC B cell numbers, NP-specific GC B cells were significantly increased in EWSR1 CKO mice (Fig. 4 *F* and *G*). Together, these findings demonstrate that EWSR1 constrains antigen-specific GC B cell responses even in the context of an immune response to a nonviral antigen.

To determine whether the enhanced GC B cell responses observed in mice with B cell–specific ablation of EWSR1 were due to increased proliferation and/or survival of GC B cells, we
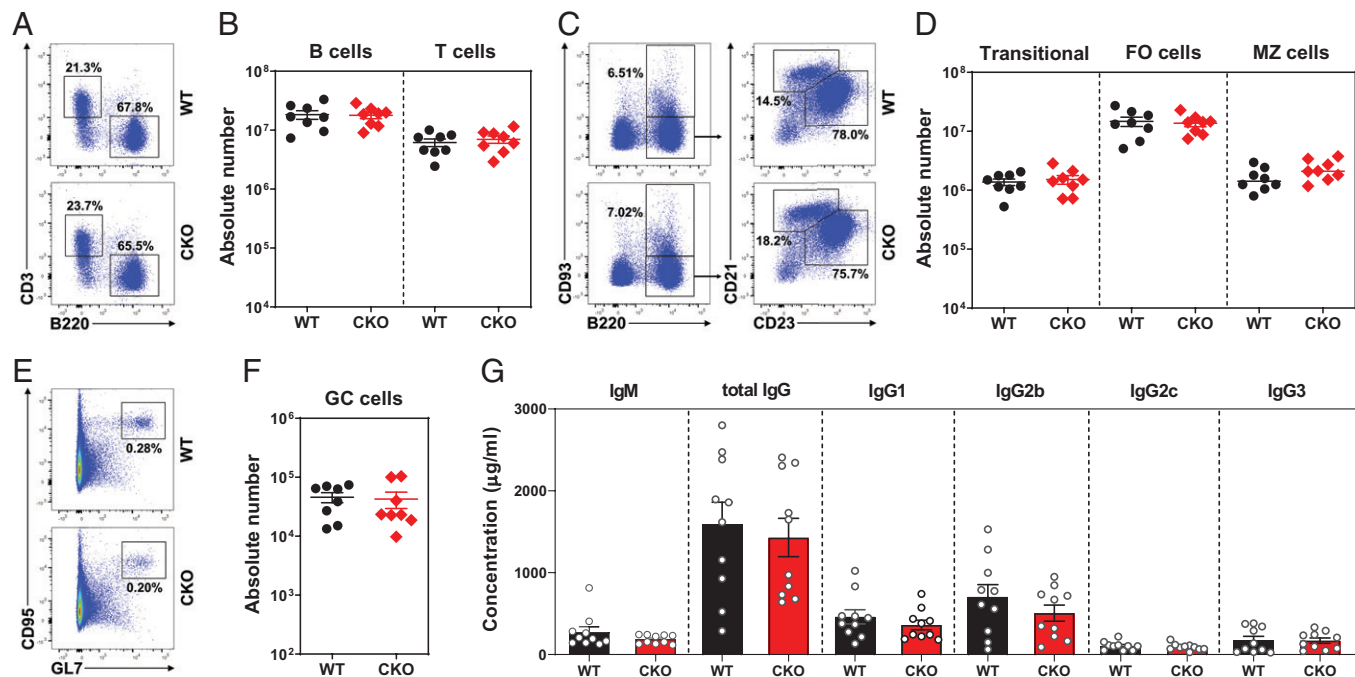
Fig. 3. EWSR1 is dispensable for peripheral B cell development and basal serum immunoglobulin production. (*A–F*) Flow cytometry was used to determine the number of T cells and B cell subsets in the spleens from 8- to 12-wk-old naïve EWSR1 WT and CKO mice. (*A*) Representative flow plots for showing the gating of B220$^+$ CD3$^-$ B cells and B220$^-$ CD3$^+$ T cells from singlets. (*B*) The number of B cells and T cells. (*C*) Representative flow plots for showing the gating of B220$^+$ CD93$^+$ transitional B cells from singlets, and the gating of CD23$^+$ FO cells and CD23$^{low/-}$ CD21$^+$ MZ cells from B220$^+$ CD93$^-$ B cells. (*D*) The number of transitional, FO, and MZ B cells. (*E*) Representative flow plots for showing the gating of GL7$^+$ CD95$^+$ GC cells from B220$^+$ B cells. (*F*) The number of GC B cells. Each symbol represents an individual mouse. The values represent the means $\pm$ the SEM of four independent experiments. (*G*) ELISA was used to quantify the levels of specific immunoglobulin isotypes (IgM, total IgG, IgG1, IgG2b, IgG2c, and IgG3) in sera from 8- to 12-wk-old naïve EWSR1 WT and CKO mice. Each dot represents an individual mouse. The values represent the means $\pm$ the SEM of three independent experiments.

quantified 5-ethynyl-2′-deoxyuridine (EdU) incorporation and the presence of active caspase 3 (aCasp3) in GC B cells at 14 d post NP-KLH immunization (Fig. 4 *H–K*). However, EWSR1-deficient GC B cells displayed no significant difference in either proliferation (Fig. 4 *H* and *I*) or apoptosis (Fig. 4 *J* and *K*) as compared with WT GC B cells. Following initial antigen activation, naïve follicular B cells enter into a Pre-GC state, characterized by up-regulated GL7 and CD38 (35–37), and undergo an initial proliferative burst prior to further differentiation (38, 39). We therefore hypothesized that EWSR1 deficiency may restrict the generation of Pre-GC B cells. To test this possibility, we analyzed Pre-GC (B220$^+$ GL7$^+$ CD38$^+$) and mature GC (B220$^+$ GL7$^+$ CD38$^-$) B cells at 14 d following NP-KLH immunization by flow cytometry (Fig. 5*A*). Intriguingly, the frequencies and numbers of both Pre-GC B cells and mature GC B cells present in EWSR1 CKO mice were significantly elevated as compared with those of EWSR1 WT control mice (Fig. 5 *B–E*). Together, these findings indicate that the enhanced GC B cell responses observed in mice with B cell–specific EWSR1 deficiency were due to increased numbers of Pre-GC B cells, demonstrating that EWSR1 constrains GC responses through regulation of Pre-GC B cells, rather than restriction of GC B cell proliferation or survival.

To determine whether the enhanced GC B cell reactions to nonviral antigen observed in EWSR1 CKO mice resulted in increased antigen-specific antibody responses, we immunized EWSR1 WT and CKO mice with NP-KLH and then determined the levels of NP-specific antibodies present in sera after 2 wk (Fig. 6). Notably, while NP-specific IgM levels were similar in both strains (Fig. 6*A*), the levels of class-switched NP-specific IgG in EWSR1 CKO mice were significantly higher than those in WT control mice (Fig. 6*B*). Consistent with the enhanced GC

reaction observed in EWSR1 CKO mice, antigen-specific class-switched antibodies including NP-specific IgG1, IgG2b, and IgG2c (but not IgG3) were strikingly elevated in immunized EWSR1 CKO mice as compared with immunized EWSR1 WT mice (Fig. 6 *C–F*). Accordingly, the number of NP-specific IgG-, IgG1-, IgG2b-, and IgG2c-secreting plasma cells was significantly increased in immunized EWSR1 CKO mice (Fig. 6 *B–E*), while the number of NP-specific IgM- and IgG3-secreting cells remained unchanged (Fig. 6 *A* and *F*). Thus, these data demonstrate that EWSR1 deficiency in B cells results in elevated antigen-specific plasma cells and antibodies. Collectively, these findings clearly demonstrate that EWSR1 constrains antigen-mediated GC B cell responses, and suggest that EWSR1 may serve as a molecular brake to limit excessive humoral immunity during T cell–dependent immune responses.

Discussion

Throughout the history of virology, in-depth studies of the mechanisms by which viruses manipulate infected cells have led to the discovery of novel host factors that regulate normal cellular processes. Similarly, in the work described here, our studies defining mechanisms by which gammaherpesvirus miRNAs manipulate infected B cells have revealed a regulatory role for the host protein EWSR1 in restricting GC B cell responses to nonviral antigens. We extend our previous studies defining *EWSR1* as a critical target for a gammaherpesvirus miRNA (23) by demonstrating that inhibition or ablation of EWSR1 in B cells significantly increased the number of gammaherpesvirus-infected GC B cells throughout the proliferative expansion phase of latency in vivo. By broadening the scope of these studies to examine GC B cell responses to a nonviral antigen
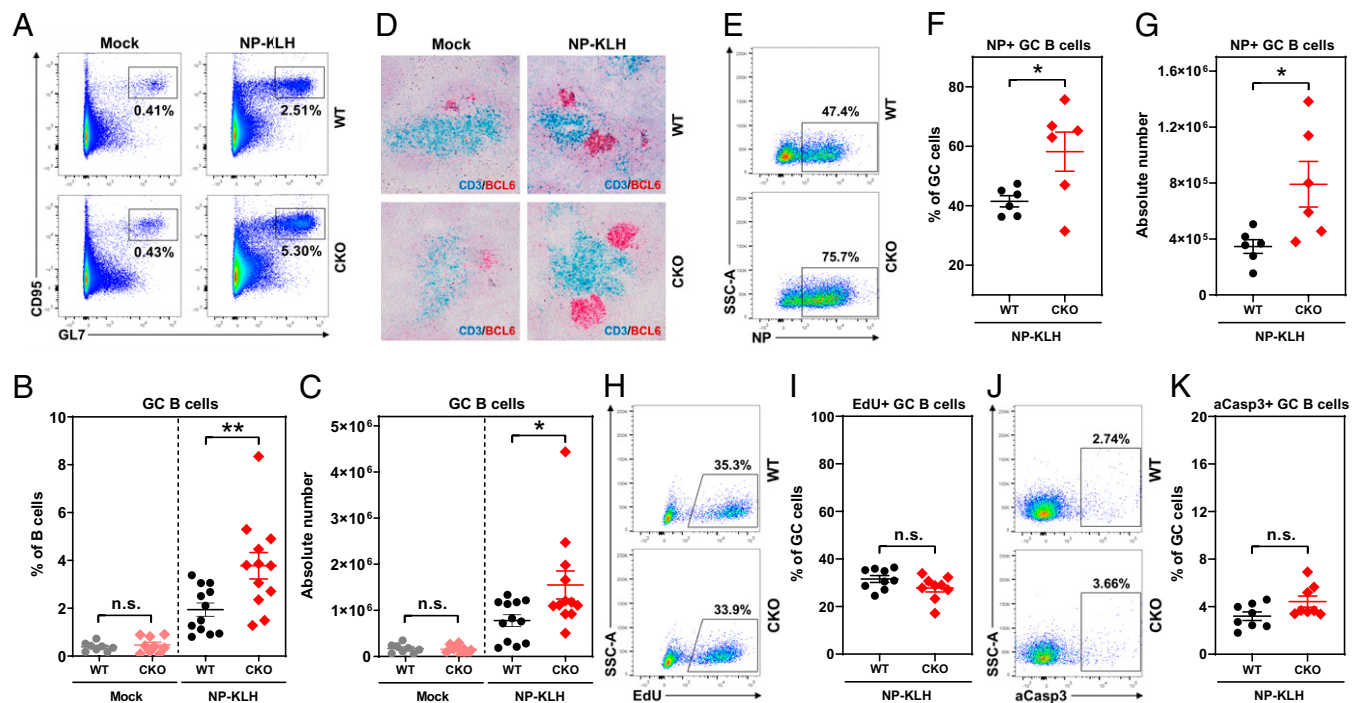
Fig. 4. B cell–specific EWSR1 deficiency enhances GC B cell response following immunization with a T cell–dependent antigen. (*A–C*) EWSR1 WT and CKO mice were mock-injected or immunized i.p. with NP-KLH, and the number of GC B cells was determined by flow cytometry at 14 d. (*A*) Representative flow plots for showing the gating of GL7$^+$ CD95$^+$ GC cells from B220$^+$ B cells. (*B*) The percentage of GC B cells. (*C*) The number of GC B cells. Each symbol represents an individual mouse. The values represent the means ± the SEM of five independent experiments. Significance was determined by a two-tailed, unpaired *t* test (*$P < 0.05$, **$P < 0.01$; n.s., not significant). (*D*) RNAScope in situ hybridization was used to stain the T cell–specific marker CD3 and the GC B cell–specific marker BCL6 on paraffin-embedded spleen sections. Representative stainings for *CD3* (blue) and *BCL6* (red) are shown. (*E–G*) EWSR1 WT and CKO mice were immunized i.p. with NP-KLH, and the percentages of NP-specific GC B cells were determined by flow cytometry at 14 d. (*E*) Representative flow plots for showing the gating of NP$^+$ cells from B220$^+$ GL7$^+$ CD95$^+$ GC B cells. (*F*) The percentage of NP-specific GC B cells. (*G*) The number of NP-specific GC B cells. Each symbol represents an individual mouse. The values represent the means ± the SEM of two independent experiments. Significance was determined by a two-tailed, unpaired *t* test (*$P < 0.05$). (*H* and *I*) Proliferation assay. EWSR1 WT and CKO mice were immunized i.p. with NP-KLH for 14 d; EdU was injected i.p. 2 h prior to spleen harvest and then the EdU incorporation was detected by flow cytometry. (*H*) Representative flow plots for gating of EdU$^+$ cells from B220$^+$ GL7$^+$ CD95$^+$ GC B cells. (*I*) The percentage of EdU$^+$ GC B cells. Each symbol represents an individual mouse. The values represent the means ± SEM of three independent experiments. Significance was determined by a two-tailed, unpaired *t* test (n.s., not significant). (*J* and *K*) Apoptosis assay. EWSR1 WT and CKO mice were immunized i.p. with NP-KLH, and the percentages of aCasp3$^+$ GC B cells were determined by flow cytometry at 14 d. (*J*) Representative flow plots for gating of aCasp3$^+$ cells from B220$^+$ GL7$^+$ CD95$^+$ GC B cells. (*K*) The percentage of aCasp3$^+$ GC B cells. Each symbol represents an individual mouse. The values represent the means ± SEM of two independent experiments. Significance was determined by a two-tailed, unpaired *t* test (n.s., not significant).

outside of the context of infection, we demonstrate that EWSR1 plays a central role in the regulation of mature B cell responses: EWSR1 deficiency in B cells resulted in a striking increase in the number of antigen-specific GC B cells and a concomitant rise in the levels of antigen-specific class-switched antibodies. B cell–specific ablation of EWSR1 did not alter proliferation or survival of GC B cells but instead resulted in the generation of increased numbers of Pre-GC B cells. Cumulatively,
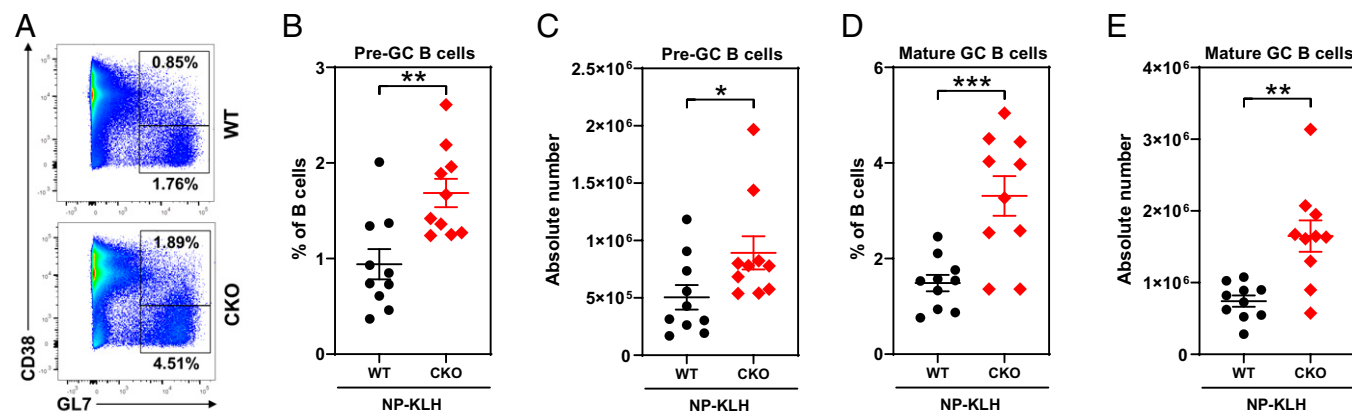

Fig. 5. B cell–specific deletion of EWSR1 promotes generation of Pre-GC B cells. EWSR1 WT and CKO mice were immunized i.p. with NP-KLH, and the numbers of Pre-GC and mature GC B cells were determined by flow cytometry at 14 d. (*A*) Representative flow plots for showing the gating of GL7$^+$ CD38$^+$ Pre-GC and GL7$^+$ CD38$^-$ mature GC cells from B220$^+$ B cells. (*B*) The percentage of Pre-GC B cells. (*C*) The number of Pre-GC B cells. (*D*) The percentage of mature GC B cells. (*E*) The number of mature GC B cells. Each symbol represents an individual mouse. The values represent the means ± SEM of two independent experiments. Significance was determined by a two-tailed, unpaired *t* test (*$P < 0.05$, **$P < 0.01$, ***$P < 0.001$).
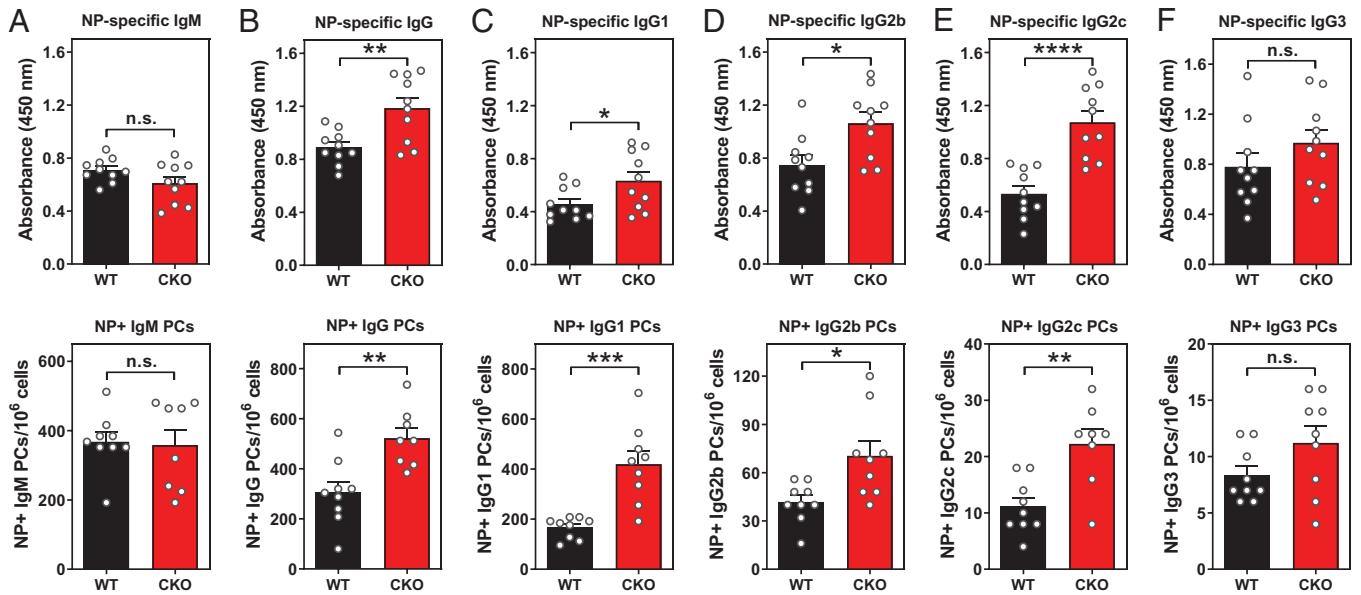
Fig. 6. B cell–specific EWSR1 deficiency enhances humoral immunity following immunization with a T cell–dependent antigen. EWSR1 WT and CKO mice were immunized i.p. with NP-KLH for 14 d; then, NP-specific antibodies in the sera were determined by ELISA, and plasma cells (PCs) secreting NP-specific antibodies in the spleens were determined by ELISpot. (*A*) The level of NP-specific IgM and the number of PCs secreting NP-specific IgM. (*B*) The level of NP-specific IgG and the number of PCs secreting NP-specific IgG. (*C*) The level of NP-specific IgG1 and the number of PCs secreting NP-specific IgG1. (*D*) The level of NP-specific IgG2b and the number of PCs secreting NP-specific IgG2b. (*E*) The level of NP-specific IgG2c and the number of PCs secreting NP-specific IgG2c. (*F*) The level of NP-specific IgG3 and the number of PCs secreting NP-specific IgG3. Each dot represents an individual mouse. The values represent the means ± the SEM of three independent experiments. Significance was determined by a two-tailed, unpaired *t* test (*$P < 0.05$, **$P < 0.01$, ***$P < 0.001$, ****$P < 0.0001$; n.s., not significant).

these findings strongly suggest that EWSR1 acts as a molecular brake at a critical checkpoint in the Pre-GC stage to constrain GC B cell reactions and thereby prevent excessive humoral immunity.

A function for EWSR1 in circulating mature B cells has not been previously reported. EWSR1 is expressed in both developing B cells in the bone marrow and mature B cells in the spleen. Although EWSR1-deficient mice typically do not survive, it has been reported that those that survive do display a subtle defect in pre–B cell development (40). However, our work suggests that this defect does not extend to the mature B cell compartment: B cell–specific deficiency of EWSR1 had no effect on 1) numbers of total mature B cells, 2) numbers of specific mature B cell subsets, or 3) basal levels of serum immunoglobulin (Fig. 3). Therefore, the signals that drive the exacerbated GC B cell responses observed here in EWSR1 CKO mice in the context of both gammaherpesvirus infection and antigen-specific B cell responses appear to be intrinsic to the activated mature B cells. These findings strongly suggest that EWSR1 functions as a negative regulator of GC B cell responses. Such a function is consistent with that of other negative regulators of B cell responses, including the protein-tyrosine phosphatase SHP1 (41), ELL (eleven-nineteen lysine-rich leukemia)-associated factor 2 (EAF2) (42), and ubiquitin-modifying enzyme A20 (43), which are essential for constraining robust B cell responses to maintain immune homeostasis and prevent autoimmune disorders.

It is notable that the enhanced GC B cell responses observed in mice with B cell–specific EWSR1 deletion were not due to enhanced proliferation or survival of GC B cells but instead correlated with an increase in generation of Pre-GC B cells. This finding is consistent with the concept that EWSR1 may govern the early proliferative burst that occurs following the initial activation of antigen-specific B cells and prior to GC entry (38, 39). Alternatively, it is plausible that EWSR1 may elevate the threshold of B cell receptor (BCR) and/or coreceptor signals required

for initial activation. This is an important distinction that will need to be clarified in future studies. Thus, it is important to note that although experiments here focused on GC B cell responses to a T cell–dependent antigen, our findings do not rule out the possibility that EWSR1 may restrict all types of mature B cell responses, or directly impact the requirement for T cell help during initial activation to the Pre-GC stage. Nevertheless, the results presented here clearly demonstrate that, at a minimum, EWSR1 restricts GC responses to a T cell–dependent antigen. These findings add EWSR1 to the growing list of host factors such as Bhlhe40 and TBK1, which, respectively, act as negative and positive regulators of Pre-GC B cell responses with no direct effect on GC B cell function (37, 44).

At present, the molecular mechanism by which EWSR1 regulates B cells is unknown. The mature B cell differentiation process, from activation of naïve follicular B cells to proliferation of Pre-GC cells to transit through the GC reaction to terminal differentiation, is highly orchestrated, requiring stepwise ratcheting of key transcription factors, antigen signaling through the BCR, and environmental cues provided by other immune cells within the milieu of the lymphoid follicle (1–4). EWSR1 is a multifunctional protein that carries out a wide range of regulatory activities including modulating transcription, RNA processing, and alternative splicing (29–31). Although EWSR1 is primarily found in the nucleus, it shuttles to the cytoplasm depending upon context. Thus, it is perhaps most plausible that EWSR1 functions to directly alter stoichiometry or isoform usage of transcription factors central to GC B cell biology, or that it directly alters B cell signaling events. For example, another negative regulator of GC B cells, A20, restricts activation of the critical transcription factor NF-κB, with A20 deficiency resulting in enhanced B cell survival and elevated numbers of GC B cells, plasma cells, and autoantibodies (43, 45). Notably, inactivation mutations in the gene encoding A20, *TNFAIP3*, are frequently associated with B cell lymphoma (46, 47). On the other hand,

the negative regulator SHP1 is a cytoplasmic tyrosine phosphatase that associates with the BCR and dephosphorylates substrates to attenuate BCR-associated signaling events, ultimately repressing GC B cell responses (48). Interestingly, though, in contrast to EWSR1, expression of SHP1 is required for maintenance of MHV68 latency, suggesting an alternative role for this protein during gammaherpesvirus infection (49). Due to the multifunctional nature of EWSR1, much work remains to define the specific mechanisms by which this interesting protein regulates GC B cell biology.

The findings presented here demonstrate a negative regulatory role for EWSR1 in constraining GC B cell responses, with EWSR1 expression restricting total numbers of Pre-GC and GC B cells, resulting in decreased plasma cell accumulation and circulating antibody levels. These results also highlight the intimate relationship of gammaherpesviruses with their B cell hosts, with these viruses evolving unique mechanisms to exploit host cell vulnerabilities. In this case, in-depth study of the ability of a viral miRNA to repress a host transcript with unknown function in B cells has revealed the importance of the host factor in regulating a central player in immune homeostasis. Thus, these findings have important potential implications for the pathogenesis of disease, as regulation of GC B cell responses is central to not only gammaherpesvirus biology but also the genesis of numerous types of B cell lymphomas and autoimmune diseases.

Materials and Methods

Cell Culture. NIH 3T12 murine fibroblasts (ATCC, CCL-164) were grown and maintained in Dulbecco's modified Eagle's medium (DMEM; Corning, 10-013-CM) supplemented with 10% fetal bovine serum (FBS; Atlanta Biologicals, S12450) and 1× penicillin-streptomycin solution (Corning, 30-002-CI) at 37 °C with 5% CO_2.

Generation of Recombinant Viruses. MHV68.H2bYFP, a recombinant marker virus that expresses eYFP under the control of the H2b promoter (18), is a phenotypically WT virus and used as the parental virus here (designated MHV68.YFP.WT). Two MHV68 *TMER5*-deficient viruses, MHV68.YFP.EWshR and MHV68.YFP.SCshR (Fig. 1*A*), in which *TMER5*-derived *pre-miR-7* and *pre-miR-12* stem loops were replaced by anti-*EWSR1* shRNAs (EW.shR #1 and EW.shR #2) or control shRNAs with scrambled sequences (SC.shR #1 and SC.shR #2), respectively, were generated on the MHV68.YFP.WT virus backbone by en passant mutagenesis, as previously described (23, 50). The anti-*EWSR1* or scrambled shRNAs have been previously described and their sequences are as follows: EW.shR #1 (5′-GACTCTGACAACAGTGCAATTTCAAGAGAATTGCACTGTTGTCAGAGTC-3′), EW.shR #2 (5′-GGAATGGTTTGATGGGAAAGATCAAGAGTCTTTCCCATCAAACCATTCC-3′), SC.shR #1 (5′-GTCAGGCTAGTAACACCTTAATCAAGAGTTAAGGTGTTACTAGCCTGAC-3′), and SC.shR #2 (5′-GAGGGTAATATGATGAGGAGTTCAAGAGACTCCTCATCATATTACCCTC-3′) (23).

Mouse Infections. Seven- to 8-wk-old C57BL/6J mice were purchased from The Jackson Laboratory, and housed at the University of Florida (Gainesville, FL) in accordance with all federal and university guidelines. All animal protocols were approved by the Institutional Animal Care and Use Committee at the University of Florida. Mice were inoculated i.n. with 10^4 plaque-forming units (PFUs) of the indicated virus in 30 μL serum-free DMEM under isoflurane anesthesia.

Flow Cytometry. For flow cytometry–based sorting of infected GC B cells expressing YFP, mice were infected i.n. with 10^4 PFUs of MHV68.YFP.WT, MHV68.YFP.SCshR, or MHV68.YFP.EWshR. At 16 dpi, spleens were harvested and single-cell suspensions were prepared as previously described (23). B cells were then isolated by immunomagnetic negative selection using an EasySep Mouse B Cell Isolation Kit (Stemcell Technologies, 19854). The cells were blocked in phosphate-buffered saline (PBS) containing 2% FBS, 0.1% sodium azide, and purified rat anti-mouse CD16/CD32 at 1:50 (BD Biosciences, 553141). The cells were then stained with specific GC B cell-surface markers

V450 rat anti-mouse CD19 at 1:200 (BD Biosciences, 560375), Alexa Fluor 647 rat anti-mouse T and B cell activation antigen GL7 at 1:200 (BD Biosciences, 561529), and PE hamster anti-mouse CD95 (BD Biosciences, 554258). Infected GC B cells (CD19$^+$ GL7$^+$ CD95$^+$ YFP$^+$) were sorted using a FACSAria II cell sorter (BD Biosciences). Sorted cells were immediately subjected to RNA extraction using an RNAqueous-Micro Kit (Ambion, AM1931) for the quantification of *EWSR1* mRNA expression level.

For flow cytometry–based quantification of total B and T cells, mature B cell subsets, GC B cells, and Pre-GC and mature GC B cells in vivo, isolated splenocytes were blocked as described above. The cells were then stained with V450 rat anti-mouse CD45R (B220) at 1:200 (BD Biosciences, 560472), APC-Cy7 hamster anti-mouse CD3e at 1:200 (BD Biosciences, 557596), PE-Cy7 rat anti-mouse CD93 at 1:200 (Thermo Fisher Scientific, 25-5892-81), APC rat anti-mouse CD21/CD35 at 1:200 (BD Biosciences, 558658), PE rat anti-mouse CD23 at 1:200 (BD Biosciences, 553139), Alexa Fluor 647 rat anti-mouse T and B cell activation antigen GL7 at 1:200 (BD Biosciences, 561529), PE hamster anti-mouse CD95 at 1:200 (BD Biosciences, 554258), PE-Cy7 hamster anti-mouse CD95 at 1:200 (BD Biosciences, 557653), or PE rat anti-mouse CD38 at 1:200 (Thermo Fisher Scientific, 12-0381-82). Identification of NP-specific GC B cells was performed by staining with NP-PE (Biosearch Technologies, N-5070-1; with a conjugation ratio of 16) at 1:100. Fluorescence-activated cell sorting acquisition was performed on a FACSCanto II or FACSymphony A3 flow cytometer (BD Biosciences). The cell subsets were gated as T cells (B220$^-$ CD3$^+$), B cells (B220$^+$ CD3$^-$), transitional B cells (B220$^+$ CD93$^+$), FO B cells (B220$^+$ CD93$^-$ CD23$^+$), MZ B cells (B220$^+$ CD93$^-$ CD23$^{low/-}$ CD21$^+$), GC B cells (B220$^+$ GL7$^+$ CD95$^+$), NP-specific GC B cells (B220$^+$ GL7$^+$ CD95$^+$ NP$^+$), Pre-GC B cells (B220$^+$ GL7$^+$ CD38$^+$), and mature GC B cells (B220$^+$ GL7$^+$ CD38$^-$). The data were analyzed using FlowJo v10 software.

qRT-PCR. RNA extracted from sorted infected GC B cells was reverse-transcribed into complementary DNA by using ProtoScript II reverse transcriptase (New England Biolabs, M0368S) with random primer mix (New England Biolabs, S1330S). The qPCR was performed in triplicate on the Bio-Rad CFX96 Touch Real-Time PCR Detection System using Maxima SYBR green/fluorescein qPCR master mix (Thermo Fisher Scientific, K0243). The primers for *EWSR1* were 5′-TATAGCACTCCAACTGCCCC-3′ and 5′-CCTGCGTTGTGGTGACTGTA-3′. Glyceraldehyde-3-phosphate dehydrogenase (GAPDH) was used as an internal control, with the primers 5′-CATGGCCTTCCGTGTTCCTA-3′ and 5′-CCTGCTTCACCACCTTCTTGAT-3′. The results were analyzed using Bio-Rad CFX Manager 3.1 software, and the *EWSR1* mRNA expression level was normalized to that of GAPDH. Relative mRNA expression changes between groups were determined by the comparative C_T method (51).

Generation of CKO Mice with B Cell–Specific EWSR1 Deficiency. The mouse line C57BL/6N-Ewsr1$^{<tm1c(EUCOMM)Wtsi>}$/TcpPtKV contains conditional *EWSR1* alleles through insertion of two loxP sites flanking exon 4 of the *EWSR1* gene (designated EWSR1$^{flox/flox}$ mice) (32, 33). CD19-Cre mice [B6.129P2(C)-Cd19$^{tm1(cre)Cgn}$/J, 006785] (34) that express the Cre recombinase gene under the control of the CD19 promoter throughout B lymphocyte development were purchased from The Jackson Laboratory. The mice with CKO of EWSR1 in B cells were generated by a two-step breeding scheme. The EWSR1$^{flox/flox}$ mice were first crossed to CD19-Cre mice to generate mice that were heterozygous for a loxP-flanked allele and heterozygous for the Cre transgene (EWSR1$^{flox/+}$ CD19$^{Cre/+}$, designated EWSR1 HET mice). Subsequently, these EWSR1 HET mice were mated back to the EWSR1$^{flox/flox}$ mice to obtain mice that were homozygous for the loxP-flanked allele and heterozygous for the Cre transgene (EWSR1$^{flox/flox}$ CD19$^{Cre/+}$, designated EWSR1 CKO mice). Littermate EWSR1$^{flox/flox}$ CD19$^{+/+}$ mice (designated EWSR1 WT mice) were used as controls in all experiments. Mouse genotypes were identified by PCR with the following primers: P1, 5′-ATTGATGTCCGAGTTTAAAAACCAT-3′, and P2, 5′-ACCTTCTATTGGATAGCACTTAAGG-3′ (Fig. 2*A*).

Western Blots. B cells were isolated from splenocytes from naïve mice as described above, and then the purity was assessed by flow cytometry. Purified B cells (>95%) were lysed with Pierce IP lysis buffer (Thermo Fisher Scientific, 87787). Cell lysates were then quantified and Western blots were performed exactly as previously described (23). The expression of EWSR1 and β-actin (as a loading control) was detected by using the primary antibodies rabbit anti-EWSR1

at 1:10,000 (Abcam, ab133288) and mouse anti–β-actin at 1:1,000 (Santa Cruz Biotechnology, sc-47778), followed by the secondary antibodies horseradish peroxidase (HRP)–conjugated goat anti-rabbit IgG at 1:5,000 (SouthernBiotech, 4050-05) and goat anti-mouse IgG at 1:5,000 (SouthernBiotech, 1010-05), respectively.

Mouse Immunizations. For a T cell–dependent immune response, 8- to 12-wk-old mice were injected i.p. with 100 μg of NP-KLH (Biosearch Technologies, N-5060-5) in Imject alum adjuvant (Thermo Fisher Scientific, 77161) at 0 and 7 d. At 14 d, spleens were harvested for flow cytometry for the evaluation of GC B cell response, and blood samples were collected for the determination of NP-specific antibody response.

RNAScope In Situ Hybridization. Spleens from mock- or NP-KLH–immunized mice were harvested at 14 d, fixed in 10% formalin, and embedded in paraffin. Determination of the T cell–specific marker CD3 and GC B cell–specific marker BCL6 in the spleen sections was performed by using the RNAScope 2.5 HD Duplex Detection Kit (Advanced Cell Diagnostics, 322500-USM) according to the manufacturer's instructions. RNA probes for *CD3* (314721) and *BCL6* (455311-C2) were purchased from Advanced Cell Diagnostics. The images were acquired using the Nikon Eclipse E600 microscope with a 10× objective and the imaging software NIS-Elements (Nikon Instruments).

Proliferation and Apoptosis Assays. For the detection of proliferating GC B cells at 14 d post NP-KLH immunization, mice were injected i.p. with EdU (MilliporeSigma, 900584) at a concentration of 50 μg/g body weight 2 h before spleen harvest. EdU incorporation was determined by the Click-iT Plus EdU Alexa Fluor 488 Flow Cytometry Assay Kit (Thermo Fisher Scientific, C10632) according to the manufacturer's instructions. For detection of apoptotic cells, aCasp3 was quantified by the CaspGLOW Fluorescein Active Caspase-3 Staining Kit (Thermo Fisher Scientific, 88-7004-42) following the manufacturer's instructions.

ELISA. For the quantification of serum immunoglobulins in naïve mice, Maxi-Sorp 96-well plates (Thermo Fisher Scientific, 442404) were coated with anti–mouse isotype-specific antibodies at 0.5 μg/mL in a carbonate/bicarbonate coating buffer (100 mM, pH 9.6). For the determination of antigen-specific antibodies in sera from immunized mice, the plates were coated with 20 μg/mL of NP(27)-BSA (bovine serum albumin; Biosearch Technologies, N-5050H). The plates were incubated at 4 °C overnight, washed with PBS containing 0.05% Tween-20 (PBST), and then blocked with PBST containing 1% BSA for 1 h at room temperature. After three washes with PBST, the plates were incubated with diluted serum samples for 2 h at room temperature. Following another three washes with PBST, the plates were incubated with HRP-conjugated goat anti-mouse isotype-specific antibodies (SouthernBiotech; IgM: 1021-05; IgG: 1015-05; IgG1: 1071-05; IgG2b: 1091-05; IgG2c: 1078-05; and IgG3: 1101-05). After a final three washes, TMB ELISA Substrate (Abcam, ab171522) was added to detect HRP enzymatic activity. The reactions were then quenched by the addition of Stop Solution for TMB Substrate (Abcam, ab171529), and the absorbance was read at 450 nm on the Promega GloMax Multi+ Detection System.

Enzyme-Linked Immunosorbent Spot Assay. Antigen-specific antibody-secreting plasma cells in the spleen from immunized mice were determined by enzyme-linked immunosorbent spot (ELISpot) assay as described previously (52). Briefly, the ELISpot plates (MilliporeSigma, MAIPS4510) were coated with 10 μg/mL of NP(27)-BSA (Biosearch Technologies, N-5050H) at 4 °C overnight. The plates were washed with PBS and blocked with DMEM containing 10% FBS at room temperature for 1 h. Splenocyte suspensions were serially twofold diluted and plated, starting with 1 million cells per well, and then incubated at 37 °C for 4 h. After washes with PBST, the plates were incubated with biotin-conjugated goat anti-mouse isotype-specific antibodies (SouthernBiotech; IgM: 1021-08; IgG: 1015-08; IgG1: 1071-08; IgG2b: 1091-08; IgG2c: 1078-08; and IgG3: 1100-08) at 4 °C overnight. The plates were washed and then incubated with ExtrAvidin-alkaline phosphatase (MilliporeSigma, E2636) for 1 h. After final washes with PBST, the plates were incubated with BCIP/NBT Liquid Substrate System (MilliporeSigma, B1911) in the dark for 5 min. The plates were washed with water and dried overnight, and then the spots were enumerated.

Statistical Analyses. All data were analyzed using Prism 9 software (GraphPad). Statistical significance was determined using a two-tailed, unpaired Student's *t* test, and *P* values less than 0.05 were considered to be statistically significant. *$P < 0.05$, **$P < 0.01$, ***$P < 0.001$, and ****$P < 0.0001$.

Data Availability. All study data are included in the article.

1. K. Basso, R. Dalla-Favera, Germinal centres and B cell lymphomagenesis. *Nat. Rev. Immunol.* **15**, 172–184 (2015).
2. N. S. De Silva, U. Klein, Dynamics of B cells in germinal centres. *Nat. Rev. Immunol.* **15**, 137–148 (2015).
3. G. D. Victora, M. C. Nussenzweig, Germinal centers. *Annu. Rev. Immunol.* **40**, 413–442 (2022).
4. J. G. Cyster, C. D. C. Allen, B cell responses: Cell interaction dynamics and decisions. *Cell* **177**, 524–540 (2019).
5. R. Küppers, Mechanisms of B-cell lymphoma pathogenesis. *Nat. Rev. Cancer* **5**, 251–262 (2005).
6. R. Küppers, R. Dalla-Favera, Mechanisms of chromosomal translocations in B cell lymphomas. *Oncogene* **20**, 5580–5594 (2001).
7. C. G. Vinuesa, I. Sanz, M. C. Cook, Dysregulation of germinal centres in autoimmune disease. *Nat. Rev. Immunol.* **9**, 845–857 (2009).
8. D. A. Thorley-Lawson, A. Gross, Persistence of the Epstein-Barr virus and the origins of associated lymphomas. *N. Engl. J. Med.* **350**, 1328–1337 (2004).
9. E. A. Mesri, E. Cesarman, C. Boshoff, Kaposi's sarcoma and its associated herpesvirus. *Nat. Rev. Cancer* **10**, 707–719 (2010).
10. H. C. Jha, S. Banerjee, E. S. Robertson, The role of gammaherpesviruses in cancer pathogenesis. *Pathogens* **5**, 18 (2016).
11. E. Barton, P. Mandal, S. H. Speck, Pathogenesis and host control of gammaherpesviruses: Lessons from the mouse. *Annu. Rev. Immunol.* **29**, 351–397 (2011).
12. Y. Wang, S. A. Tibbetts, L. T. Krug, Conquering the host: Determinants of pathogenesis learned from murine gammaherpesviruses. *Annu. Rev. Virol.* **8**, 349–371 (2021).
13. H. W. Virgin IV *et al.*, Complete sequence and genomic analysis of murine gammaherpesvirus 68. *J. Virol.* **71**, 5894–5904 (1997).
14. N. P. Sunil-Chandra, J. Arno, J. Fazakerley, A. A. Nash, Lymphoproliferative disease in mice infected with murine gammaherpesvirus 68. *Am. J. Pathol.* **145**, 818–826 (1994).
15. V. L. Tarakanova *et al.*, Murine gammaherpesvirus 68 infection is associated with lymphoproliferative disease and lymphoma in BALB β2 microglobulin-deficient mice. *J. Virol.* **79**, 14668–14679 (2005).
16. D. A. Thorley-Lawson, Epstein-Barr virus: Exploiting the immune system. *Nat. Rev. Immunol.* **1**, 75–82 (2001).
17. J. E. Roughan, D. A. Thorley-Lawson, The intersection of Epstein-Barr virus with the germinal center. *J. Virol.* **83**, 3968–3976 (2009).
18. C. M. Collins, S. H. Speck, Tracking murine gammaherpesvirus 68 infection of germinal center B cells in vivo. *PLoS One* **7**, e33230 (2012).
19. E. Flaño, S. M. Husain, J. T. Sample, D. L. Woodland, M. A. Blackman, Latent murine γ-herpesvirus infection is established in activated B cells, dendritic cells, and macrophages. *J. Immunol.* **165**, 1074–1081 (2000).
20. E. Flaño, I.-J. Kim, D. L. Woodland, M. A. Blackman, γ-herpesvirus latency is preferentially maintained in splenic germinal center and memory B cells. *J. Exp. Med.* **196**, 1363–1372 (2002).
21. M. R. Fabian, N. Sonenberg, W. Filipowicz, Regulation of mRNA translation and stability by microRNAs. *Annu. Rev. Biochem.* **79**, 351–379 (2010).
22. D. P. Bartel, Metazoan microRNAs. *Cell* **173**, 20–51 (2018).
23. Y. Wang, E. R. Feldman, W. L. Bullard, S. A. Tibbetts, A gammaherpesvirus microRNA targets EWSR1 (Ewing sarcoma breakpoint region 1) in vivo to promote latent infection of germinal center B cells. *mBio* **10**, e00996-19 (2019).
24. J. C. Schwartz, T. R. Cech, R. R. Parker, Biochemical properties and biological functions of FET proteins. *Annu. Rev. Biochem.* **84**, 355–379 (2015).
25. J. Lee *et al.*, EWSR1, a multifunctional protein, regulates cellular function and aging via genetic and epigenetic pathways. *Biochim. Biophys. Acta Mol. Basis Dis.* **1865**, 1938–1945 (2019).
26. O. Delattre *et al.*, Gene fusion with an ETS DNA-binding domain caused by chromosome translocation in human tumours. *Nature* **359**, 162–165 (1992).
27. H. Kovar, Dr. Jekyll and Mr. Hyde: The two faces of the FUS/EWS/TAF15 protein family. *Sarcoma* **2011**, 837474 (2011).
28. M. P. Paronetto, Ewing sarcoma protein: A key player in human cancer. *Int. J. Cell Biol.* **2013**, 642853 (2013).
29. W. J. Law, K. L. Cann, G. G. Hicks, TLS, EWS and TAF15: A model for transcriptional integration of gene expression. *Brief. Funct. Genomics Proteomics* **5**, 8–14 (2006).
30. A. Y. Tan, J. L. Manley, The TET family of proteins: Functions and roles in disease. *J. Mol. Cell Biol.* **1**, 82–92 (2009).
31. M. P. Paronetto, B. Miñana, J. Valcárcel, The Ewing sarcoma protein regulates DNA damage-induced alternative splicing. *Mol. Cell* **43**, 353–368 (2011).
32. H. Tian, T. Billings, P. M. Petkov, EWSR1 affects PRDM9-dependent histone 3 methylation and provides a link between recombination hotspots and the chromosome axis protein REC8. *Mol. Biol. Cell* **32**, 1–14 (2021).
33. H. Tian, P. M. Petkov, Mouse EWSR1 is crucial for spermatid post-meiotic transcription and spermiogenesis. *Development* **148**, dev199414 (2021).
34. R. C. Rickert, J. Roes, K. Rajewsky, B lymphocyte-specific, Cre-mediated mutagenesis in mice. *Nucleic Acids Res.* **25**, 1317–1318 (1997).

35. J. J. Taylor, K. A. Pape, M. K. Jenkins, A germinal center-independent pathway generates unswitched memory B cells early in the primary response. *J. Exp. Med.* **209**, 597–606 (2012).

36. J. L. Johnson *et al.*, The transcription factor T-bet resolves memory B cell subsets with distinct tissue distributions and antibody specificities in mice and humans. *Immunity* **52**, 842–855.e6 (2020).

37. M. S. J. Lee *et al.*, B cell-intrinsic TBK1 is essential for germinal center formation during infection and vaccination in mice. *J. Exp. Med.* **219**, e20211336 (2022).

38. T. D. Chan *et al.*, Antigen affinity controls rapid T-dependent antibody production by driving the expansion rather than the differentiation or extrafollicular migration of early plasmablasts. *J. Immunol.* **183**, 3139–3149 (2009).

39. F. Coffey, B. Alabyev, T. Manser, Initial clonal expansion of germinal center B cells takes place at the perimeter of follicles. *Immunity* **30**, 599–609 (2009).

40. H. Li *et al.*, Ewing sarcoma gene EWS is essential for meiosis and B lymphocyte development. *J. Clin. Invest.* **117**, 1314–1323 (2007).

41. L. I. Pao *et al.*, B cell-specific deletion of protein-tyrosine phosphatase Shp1 promotes B-1a cell development and causes systemic autoimmunity. *Immunity* **27**, 35–48 (2007).

42. Y. Li *et al.*, EAF2 mediates germinal centre B-cell apoptosis to suppress excessive immune responses and prevent autoimmunity. *Nat. Commun.* **7**, 10836 (2016).

43. R. M. Tavares *et al.*, The ubiquitin modifying enzyme A20 restricts B cell survival and prevents autoimmunity. *Immunity* **33**, 181–191 (2010).

44. R. Rauschmeier *et al.*, Bhlhe40 function in activated B and TFH cells restrains the GC reaction and prevents lymphomagenesis. *J. Exp. Med.* **219**, e20211406 (2022).

45. N. Hövelmeyer *et al.*, A20 deficiency in B cells enhances B-cell proliferation and results in the development of autoantibodies. *Eur. J. Immunol.* **41**, 595–601 (2011).

46. M. Kato *et al.*, Frequent inactivation of A20 in B-cell lymphomas. *Nature* **459**, 712–716 (2009).

47. M. Compagno *et al.*, Mutations of multiple genes cause deregulation of NF-kappaB in diffuse large B-cell lymphoma. *Nature* **459**, 717–721 (2009).

48. A. M. Khalil, J. C. Cambier, M. J. Shlomchik, B cell receptor signal transduction in the GC is short-circuited by high phosphatase activity. *Science* **336**, 1178–1181 (2012).

49. K. E. Johnson *et al.*, B cell-intrinsic SHP1 expression promotes the gammaherpesvirus-driven germinal center response and the establishment of chronic infection. *J. Virol.* **94**, e01232-19 (2019).

50. E. R. Feldman *et al.*, Virus-encoded microRNAs facilitate gammaherpesvirus latency and pathogenesis in vivo. *mBio* **5**, e00981-14 (2014).

51. T. D. Schmittgen, K. J. Livak, Analyzing real-time PCR data by the comparative C(T) method. *Nat. Protoc.* **3**, 1101–1108 (2008).

52. E. K. Moser *et al.*, The E3 ubiquitin ligase Itch restricts antigen-driven B cell responses. *J. Exp. Med.* **216**, 2170–2183 (2019).